JOURNAL OF MATERIALS SCIENCE 33 (1998) 1189–1199

# Plasma-assisted deposition of metal and metal oxide coatings

H. AKBULUT
*Sakarya University, Engineering Faculty, Department of Metallurgy, Esentepe Campus, Sakarya 54040, Turkey*

O. T. INAL
*Materials and Metallurgical Engineering, New Mexico Tech, Socorro, NM 87801, USA*

A combination of physical vapour deposition and plasma-assisted chemical vapour deposition techniques were used to deposit Cu-, Ni- and Sn-rich $SnO/SnO_2$ coatings on metal and ceramic substrates. Cu and Ni were deposited on Al alloy 6061 substrates and Ni deposition was also performed on glass microscope slides and commercially pure alumina substrates. Sn-rich $SnO/SnO_2$, on the other hand, was coated on stainless steel and pure Cu substrates. A direct-current plasma system was used to deposit the pure metals in vacuum with a resistively heated tungsten boat that was coated with alumina. All samples were sputtered for 20 min in an argon : hydrogen (1 : 1) atmosphere at a pressure of 300 mTorr. To reduce contamination and oxidation of both substrates and deposited layers, Cu and Ni coatings were made with argon:hydrogen (2 : 1) carrier gas. Sn-rich tin oxide coatings were deposited in a pure argon atmosphere (no hydrogen) to allow for the oxidation of Sn deposits on the stainless steel and copper substrates. Investigations of coated surfaces by scanning electron microscopy and X-ray diffraction showed coatings to be smooth, continuous and pure. Deposition rates showed this application to provide a very high rate when compared with chemical vapour deposition and metal–organic chemical vapour deposition techniques. Scratch tests results prove good attachment of the coatings to their respective substrates. © *1998 Chapman & Hall*

## 1. Introduction

Metallization in advanced integrated circuit (IC) devices is gaining increased importance with increasing device density and decreasing feature sizes because the performance of the total system is dominated by the interconnections [1, 2]. Aluminium (Al) and Al alloys are widely used as metallization in very-large-scale integrated (VLSI) circuit processing at present. However, pure Al has serious limitations in submicron devices owing to its low electromigration resistance, hillock formation and stress-induced void formation. To improve such performance limitations Al alloys are used, but these alloys show relatively high resistivity. Thus other metallization materials are being studied as candidates to replace Al and Al-alloys in these applications [3].

Thin films of conductive materials are also being investigated, or employed, for the metallization of microelectronic chips and for packaging metallization to produce specific interconnection networks in customized microelectronics devices [4, 5]. In recent years, copper (Cu) and nickel (Ni) metallizations have been seen to be adequate replacement for Al in portions of the interconnect scheme [3]. Cu is a material which, compared with Al, has favourably low resistivity and electromigration properties. Among common materials that are conductive such as Au and Ag, Cu is the least expensive and thus amenable for industrial use. Thin films of Cu, therefore, have attracted much interest lately, in this regard. Consequently, the past 5 years have witnessed an explosive growth Cu in the use of Cu VLSI circuits [5].

Ni-coated glass and metallic substrates are also being used in the microelectronics industry. In producing ceramic tube capacitors, the inside and outside of the tubes are coated with Ni [6]. The deposition of Ni has generally been carried out by laser breakdown of metal alkyls and metal carbonyls [7]. The present attempt, which utilized direct current plasma deposition, is quite unique in this regard and should offer an alternative to these procedures.

Transparent conductive oxide films have found application in numerous electronic devices as well. These include solid-state image sensors, solar cells and large-area information displays of a number of materials. Tin oxide is one of the most common among these and is capable of meeting the constrasting specifications of high optical transmittivity and low specific resistivity [8]. Tin-oxide-based coatings are also some of the semiconducting materials that are

widely used for sensing, oxidizing and reducing gases. This is due to their sensitivity to small concentrations of gas [9].

Coatings on metallic and ceramic materials that are subjected to severe working conditions allow reduced atmospheric interactions and increased corrosion resistance. These resistances can only be achieved with proper adhesion of the coating to its substrate. Among various techniques used to evaluate adhesion, the scratch test appears to be quite practical and reliable for metallic and ceramic coatings [10]. In the scratch test, a loaded diamond stylus is drawn over the coated surface under a progressively increasing normal force. The critical load is defined as the load at which the coated film is removed from the substrate. The critical load is determined in conjunction with observations utilizing optical microscopy or scanning electron microscopy (SEM). The adhesion measurements of coatings deposited in the present study, were made with this technique.

The intent of the present study was to produce thick metal and metal oxide layers on metallic and ceramic substrates by combining physical vapour deposition (PVD) and plasma-assisted chemical vapor deposition (PACVD) techniques in a direct-current (d.c.) plasma system. Subsequently, the resultant microstructure and adhesion of the coatings were elucidated through SEM, X-ray diffraction (XRD) and scratch test methods, respectively.

## 2. Experimental procedure

The substrates used, in the present work, were commercial Al alloy 6061, glass microscope slides, commercially pure alumina, type 304 stainless steel and electronic-grade Cu. Cu, stainless steel and Al substrates were prepared through mechanical polishing (with emery paper grades of 240–320–400–600) and a subsequent rinse in distilled water and final cleaning with methanol. Al alloy 6061 substrates were additionally subjected to chemical etching, with Keller's reagent for 2 min, to remove contamination and unavoidable oxide layer prior to placement in the chamber and subsequent evacuation. Glass and alumina substrates were rinsed with distilled water and then cleaned with methanol prior placement in the vacuum system and argon gas sputtering. A d.c. plasma system was used for the coating of metallic and ceramic substrate surfaces with pure metal or metal-rich oxide layers. The details of the plasma apparatus as well as the uniqueness of plasma-assisted surface processing have been given elsewhere [11]. For all coatings, the system was evacuated to $10^{-3}$ Torr pressure previous to sputtering with the carrier gas mixture. A tungsten boat, coated with alumina, and amenable to resistive heating, was used as the source for metal vapours inside the vacuum system. All the metals evaporated were of electronic-grade purity.

Following placement in the vacuum chamber, each sample was subjected to ion bombardment, sputter cleaning, in an argon and hydrogen (1:1) atmosphere at a gas pressure of 300 mTorr and a cathodic voltage of 900 V for 20 min. The sputtering of the substrates were made at a substrate temperature of 300–450 °C, depending on the materials coated. The substrates were then coated with Cu. Ni or tin (Sn)-rich tin oxide. It was reported that, in the absence of $H_2$, the metallic films usually contain significant amounts of impurities [12]. To decrease the impurities and increase deposition rate, all metallic coatings, except for $Sn/SnO–SnO_2$ films, an $Ar:H_2$ (2:1) gas mixture was used to provide a clean coating on the metal and ceramic substrates. The substrates and associated coating variables are summarized in Table I.

All coatings were investigated for layer thickness, as measured by metallography following grinding and polishing of the samples by conventional methods. For good edge retention, coated samples were mounted in bakelite with SiC particles. SEM analysis was carried out on a Hitachi HHS-2R system employing a 20 KeV electron beam. The grain size and grain size distribution of the coatings were determined from scanning electron micrographs.

Scratch testing was performed using a Romulus III universal scratch tester (dead load) fitted with a diamond stylus of a radius of 533 μm. At least four scratches were performed on a given sample. Normal loads, effective friction, transverse loads and acoustic emission outputs were recorded by a computer, attached to the scratch tester. A standard loading speed of 0.15 N $min^{-1}$ was used, the scratches being about 2.5–4.0 mm long depending on the material that had to be scratch tested. The displacements were obtained by a manually operated micrometer screw, allowing one to make a series of parallel scratches on the same sample. The shapes and the scratch channels were studied by optical microscopy and SEM. The coating failure, $L_c$, was estimated by using the information obtained from microscopic observations and from the data on acoustic emission and effective friction.

TABLE I The experimental conditions for the deposition of plasma-assisted metal and metal oxide coatings

| Coating | Substrate | Substrate temperature (°C) | Deposition time (min) | Pressure (mTorr) | Gas mixture $Ar:H_2$ | Filament temperature (°C) |
|---|---|---|---|---|---|---|
| Cu | Al alloy 6061 | 300 | 4 | 300 | 2:1 | 1500 |
| Ni | Al alloy 6061 | 300 | 4 | 300 | 2:1 | 1600 |
| Ni | Glass | 450 | 6 | 300 | 2:1 | 1800 |
| Ni | $Al_2O_3$ | 450 | 6 | 300 | 2:1 | 1800 |
| Sn | Stainless steel | 350 | 4 | 300 | Ar | 1450 |
| Sn | Cu | 300 | 4 | 300 | Ar | 1400 |

TABLE II A summary of experimental results of metal and metal oxide coatings on the different metal and ceramic substrates

| Coating | Substrate | Thicknes (μm) | Grain size (μm) | Deposition rate ($nm\,min^{-1}$) | $L_c$ ($N$) |
|---|---|---|---|---|---|
| Cu | Al | $6 \pm 1.1$ | $0.64 \pm 0.3$ | 1500 | $887 \pm 2.2$ |
| Ni | Al | $4 \pm 0.8$ | $0.33 \pm 0.02$ | 750 | $9.75 \pm 1.9$ |
| Ni | Glass | $8 \pm 0.2$ | $0.48 \pm 0.02$ | 1333 | $4.63 \pm 0.8$ |
| Sn | Cu | $6 \pm 0.3$ | $0.56 \pm 0.06$ | 1500 | $10.5 \pm 1.7$ |
| Sn | Stainless steel | $7 \pm 0.4$ | $1.08 \pm 0.25$ | 1500 | $7.5 \pm 1.4$ |
| Ni | $Al_2O_3$ | — | $0.51 \pm 0.03$ | | — |

## 3. Results and discussion

### 3.1. Results

The results of the characterization of all coatings investigated are summarized in Table II which contains the values of the thickness of the coatings, grain sizes, deposition rates and mean critical load, $L_c$.

#### *3.1.1. Surface structure*

Scanning electron micrographs of Cu and Ni coatings on Al alloy 6061 are shown in Fig. 1, showing a continuous smooth polycrystalline structure and a uniform, dense surface with a grain size of 0.62–0.66 μm for Cu and 0.32–0.36 μm for Ni. As shown in the figure, the Ni-coated surface exhibits a finer grain size than does the Cu-coated surface on the same substrate. Fig. 2 presents Ni coating structure deposited on coventional glass microscope slides and commercially pure alumina substrates. As shown in Fig. 2a, Ni particles showed a triangular prismatic shape on the glass substrates with a mean size of 0.40 μm, whereas Ni on the alumina surface gives very fine equiaxed droplets of Ni (Fig. 2b). Fig. 3, on the other hand, presents the surface structure of Sn coating on the stainless steel (Fig. 3a) and on the pure Cu substrates (Fig. 3b). A Sn coating on a Cu substrate showed a finer grain size than did a Sn coating on type 304 stainless steel. The deposit structure on the stainless steel shows a very large particle size distribution (between 0.8 and 1.35 μm) and some of the particles have coalesced, probably because of the high substrate temperature.

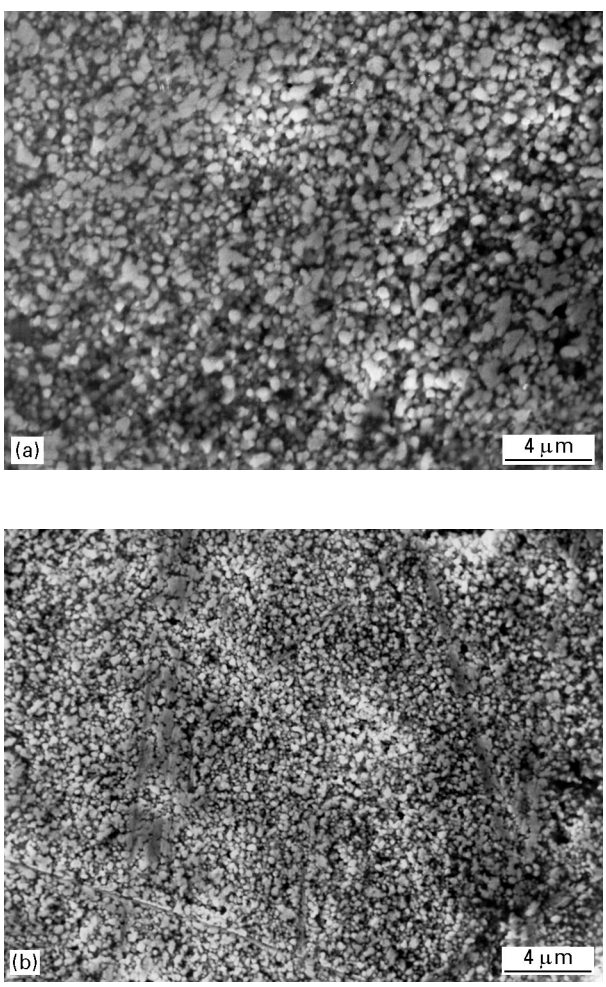


*Figure 1* Scanning electron micrographs of surface morphologies of Cu and Ni coatings, deposited on an Al alloy 6061 substrate at 300 mTorr total gas pressure and 300 °C substrate temperature: (a) Cu deposit; (b) Ni deposit.

#### *3.1.2. X-ray diffraction results*

The XRD patterns of Cu films deposited on Al alloy 6061 substrates exhibited only the diffraction peaks corresponding to Cu cubic phase (Fig. 4a). In particular, diffraction peaks ascribable to $Cu_2O$ or CuO phases were never detected in the XRD data. XRD patterns showed a clean Cu phase with major diffraction peaks appearing at $2\theta = 43.220^\circ$ (1 1 1), $51.945^\circ$ (2 0 0), $784.100^\circ$ (2 2 0) and $92.455^\circ$ (3 1 1). The XRD pattern for Ni coatings on the Al alloy 6061 substrate (Fig. 4b) showed main diffraction peaks at $2\theta = 43.955^\circ$ (1 1 1), $50.299^\circ$ (2 0 0), $74.100^\circ$ (2 2 0) and $89.700^\circ$ (3 1 1) and no NiO peak was detected. The XRD patterns of Ni coatings on glass and alumina are presented in Fig. 5a and b, respectively. A relatively high-intensity NiO peak is observed on glass substrate coated with Ni. The XRD pattern of Ni-coated alumina sample also showed a NiO peak at $2\theta = 43.331^\circ$, but the amount of NiO phase on the alumina substrate is much less than the NiO on the glass surface. Fig. 6a and b shows the XRD patterns of Sn-coated stainless steel and Cu samples, respectively. To obtain Sn-rich tin oxide coating, $H_2$ gas was not used in the plasma system and the deposited particles were allowed to oxidize in a controlled manner. Therefore, the XRD patterns of both stainless steel and Cu substrates coated with Sn showed small quantities of SnO and $SnO_2$.

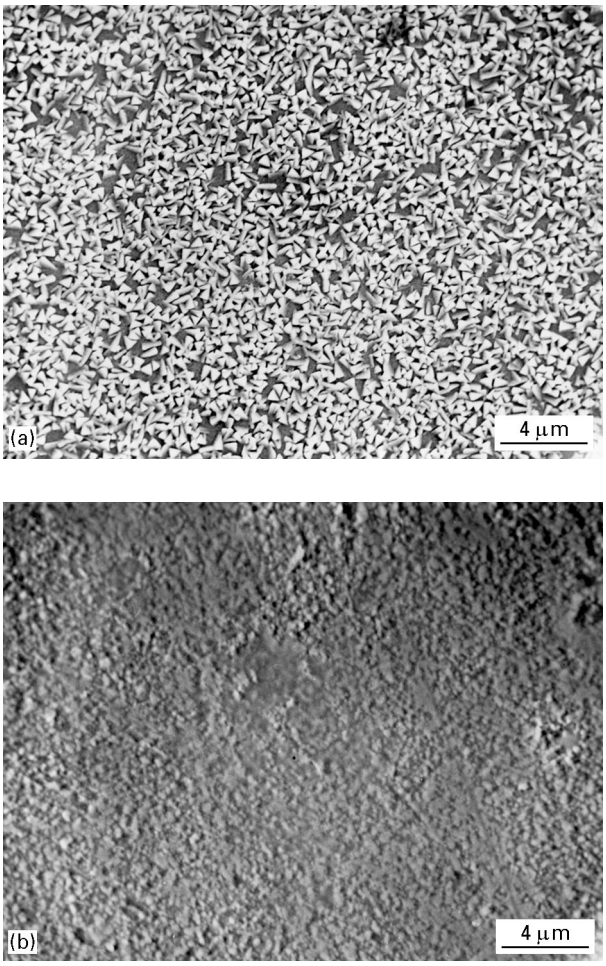


*Figure 2* Scanning electron micrographs of surface morphologies of Ni coatings, deposited at 300 mTorr total gas pressure and 450 °C substrate temperature: (a) Ni deposit on glass microscope slide; (b) Ni deposit on alumina substrates.

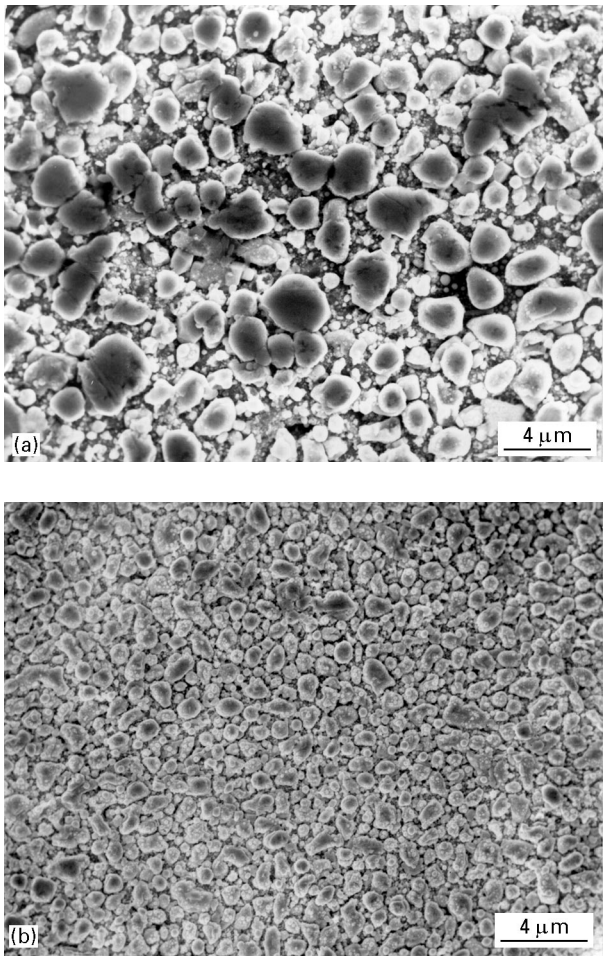


*Figure 3* Scanning electron micrographs of surface morphologies of Sn-rich, tin oxide coatings deposited at 300 mTorr total gas pressure: (a) coating on type 304 stainles steel (substrate temperature 350 °C); (b) coating on Cu (substrate temperature, 300 °C).

### 3.1.3. Scratch test results

Typical scratch test curves for the coating/substrate combinations are shown in Figs 7–10. The scratch test graphics contain applied normal load (in newtons), effective friction, transverse load (in newtons) and acoustic emission curves. Fig. 7 presents the scratch test results for Cu and Ni-coated Al alloy 6061 substrates, and Fig. 8 shows Ni-coated glass and alumina sample scratch test results. Fig. 9, on the other hand, illustrates the scratch test results for Sn-coated stainless steel and Cu substrates. As shown in Fig. 7, the scratch test results are very similar for Cu and Ni coatings on the Al alloy 6061 substrates and they give approximately the same values of the critical force, $L_c$. On the rough surface of the alumina substrates, the coating thickness and the critical force values could not be detected by traditional microscopy techniques. As shown in Table II, the Sn coatings on Cu substrates give better critical force values than do those of stainless steel. To compare adhesion properties of traditional electroless Ni coating on Al alloy 6061 with a plasma-assisted Ni coating on the same material, Ni was coated on the Al alloy 6061 surface using electroless coating at the same thickness as the plasma-coated alloy. As shown in Fig. 7b and Fig. 10, the critical force, $L_c$, of the plasma-assisted Ni coating is approximately 10 N whereas electroless Ni-coated material gives an $L_c$ value of only 2.5 N, which is a quarter of that of a plasma-assisted coating of Ni on the same substrate.

The scanning electron micrographs of typical scratch tracks of the coatings are illustrated in Fig. 11. Since the scratch channels are very similar, only a Cu-coated surface is given for Al alloy 6061 substrates that were coated with both Cu and Ni. The critical loads for Cu- and Ni-coated Al alloy 6061 substrate samples could not be detected by optical microscopy inspections, even at high magnifications, on the scratch channels; SEM, however, did not show any microcracks. The critical loads for these two coatings were estimated from the effective friction and acoustic emission curves. Similarly, the scratch channel of Ni-coated glass (Fig. 12) is given as an example for Ni-coated ceramics. For a given load, a rapid increase in acoustic emission is observed and for the Ni coating this can be correlated to adhesive failure of the coating (Ni)–substrate (glass) interface. These adhesive failures appear as areas of uncovered substrate in the track and small chips along its edges. This is similar to the regular chipping along the edge of the scratch track that is often used as a measure of the critical load, $L_c$ for creating detachment [13]. Scratch channels of the Ni coating on the glass substrate were investigated by

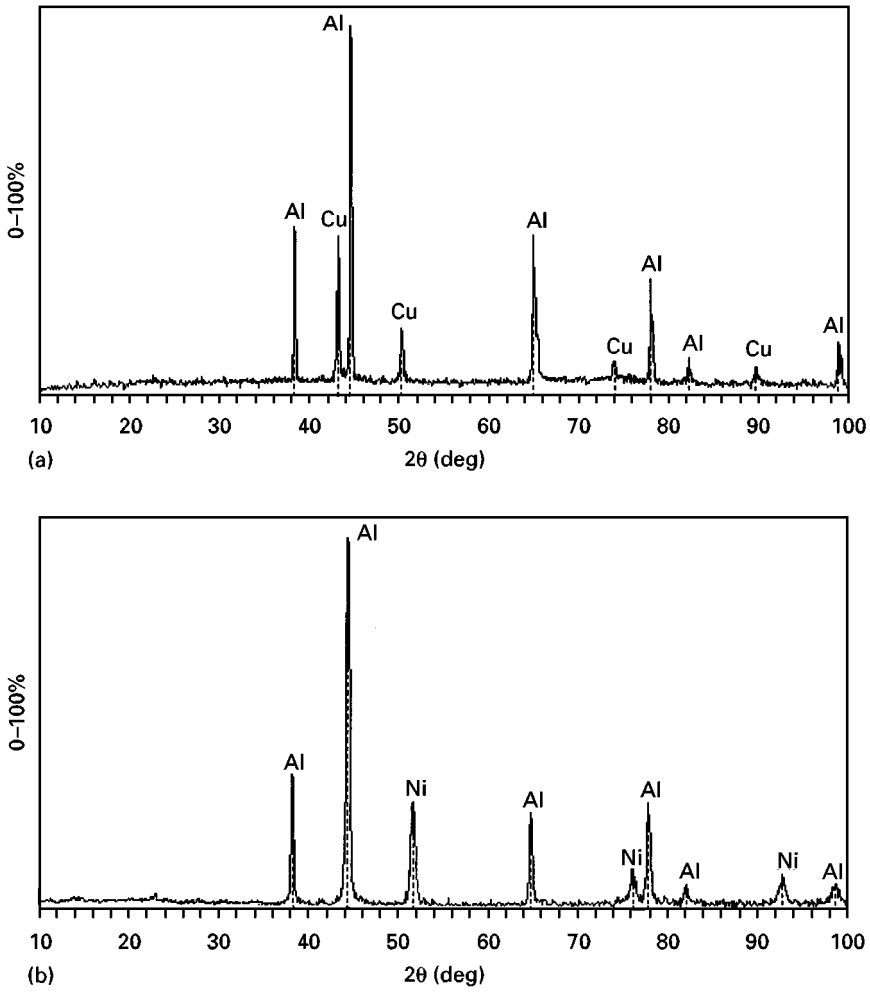


*Figure 4* XRD patterns of (a) Cu and (b) Ni, deposited on Al alloy 6061 substrates.

SEM, under a high magnification. Fig. 13 shows the inside of the scratch channel that exhibited small cracks, related to Ni cracking, after extensive plastic deformation.

Among the Sn-coated materials, the stainless steel substrate was chosen to represent Sn-rich tin oxide coatings for scratch traces (Fig. 14). As shown in Fig. 14, the scratch tracks exhibit a large amount of plastic deformation.

## 4. Discussion

Most metal deposition processes can be divided into PVD and chemical vapour deposition (CVD)-type processing [3]. The most common techniques that are being used for metallization are the CVD and (MOCVD) [14]. Laser-assisted chemical vapour deposition (LCVD) is another metallization technique applied especially for Ni [15, 16], Pt and metal oxides such as $TiO_2$ [17]. Traditionally, Cu and Ni films have been deposited by electroless coating [18] or electron beam evaporation. However, these deposition techniques suffer from inadequate step coverage; this often results in the formation of microcracks and discontinuities at holes and deep trenches [19]. In recent years, CVD and MOCVD techniques have been used for Cu metallization of advanced IC devices. Both CVD and MOCVD techniques show slower deposition rates when compared with rates obtained in the present study (Table II). In addition, a high rate of contamination of Cu films by carbon-based impurities has been observed in the coating deposited with these latter two techniques [20]. Using these two techniques, the increase in coating thickness is also limited because of the oxidation of the thin films by the increase in the deposition time. The CVD-processed Ni coatings, in addition, have received much less attention for the metallization of IC or semiconductor devices; since Ni halides are not volatile, reactive plasma processing based on halide chemistry, currently used in the manufacture of ICs, cannot be employed for the dry etching of Ni films [21]. In the present case, the Ni coating rates and the high purities achieved obviated the need for high-vacuum systems. Laser deposition and LCVD processes are of interest for low-temperature overlayer production. For Ni coating by LCVD, in general, Ni carbonyl and Ni hydryl precursors have been used [15]. The LCVD rate is seen to eventually be limited by diffusion of reactants to the reaction zone and also be laser-induced convection. These limiting factors are seen to be functions of the initial concentration of reactants and inert species and the surface and gas temperatures; LCVD of Ni, from $Ni(CO)_4$, has been

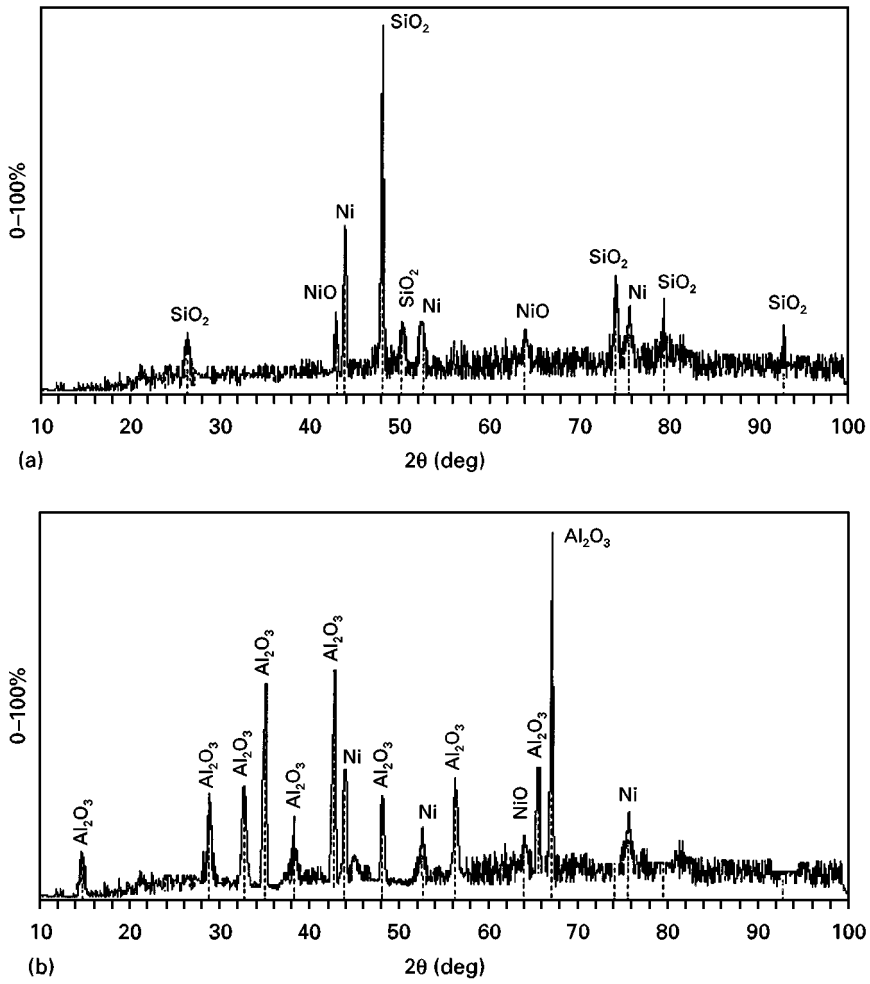


*Figure 5* XRD patterns: (a) Ni deposited on a glass microscope slide; (b) Ni deposited on an alumina substrate.

performed using irradiated areas of several microns diameter [22].

PACVD is a technique which offers the ability to deposit overlayers on geometrical complex-shaped subtrates. This ability is of great importance when, for instance, random shaped parts need to be coated. Large numbers of small ceramic tubes have also been coated uniformly in bulk processes on both the inside and the outside with a metallic conductor [6]. The mass transport in CVD or PACVD can be considered a two-step process: first, the transport of reactants in the gas phase and their formation on the substrate by diffusion, and secondly, the decomposition of the reactants at the substrate surface. Either process can be rate limiting. In the present work, Cu, Ni and Sn depositions on the different substrates were carried out using a combination of PVD and PACVD. A d.c. plasma was used to enhance the deposition rate and the adhesion quality of vaporized metallic species.

During the coating of the substrates with Ni, Cu and Sn, Ar and $H_2$ ions bombard the surface of the substrates, performing a sputter etch. This effectively cleans the surface for the ensuing coating process. The sputtering continues during the deposition as well. This greatly improves the adhesion properties of the films [11].

It has been reported that the temperature and the carrier gas composition are the major factors that control the film purity in CVD-coated Cu films. Most workers have reported deposition temperatures in the range 250–400 °C for the coating of Cu [3]. Based on Auger electron spectroscopy (AES) measurements, it has been concluded that $H_2$ must be present in the carrier gas to obtain pure films when organometallic Cu precursors are used [20]. As in the case of PACVD, it is thought that using $H_2$ carrier gas, together with Ar, is necessary to obtain pure coating layers. Since the vacuum level of the plasma system used in present work was relatively low ($10^{-3}$ Torr), a 1:1 Ar:$H_2$ plasma gas ratio was used in sputtering and a 2:1 Ar:$H_2$ ratio was used during Cu and Ni coating.

To increase the deposition rate of the metallic coatings, by CVD–PACVD or LCVD, the substrate temperatures should be increased but, at high substrate temperatures, the Cu films have shown high resistivity which is explained by the presence of oxygen. Awaya and Arita [19] reported that $H_2$ carrier gas is essential to produce low-resistivity Cu films. They also report that $H_2$ is mainly responsible for reducing contamination, such as carbon impurities. In the present work, XRD results did not show any oxidation for Cu and Ni coatings on the Al alloy 6061 substrates. The

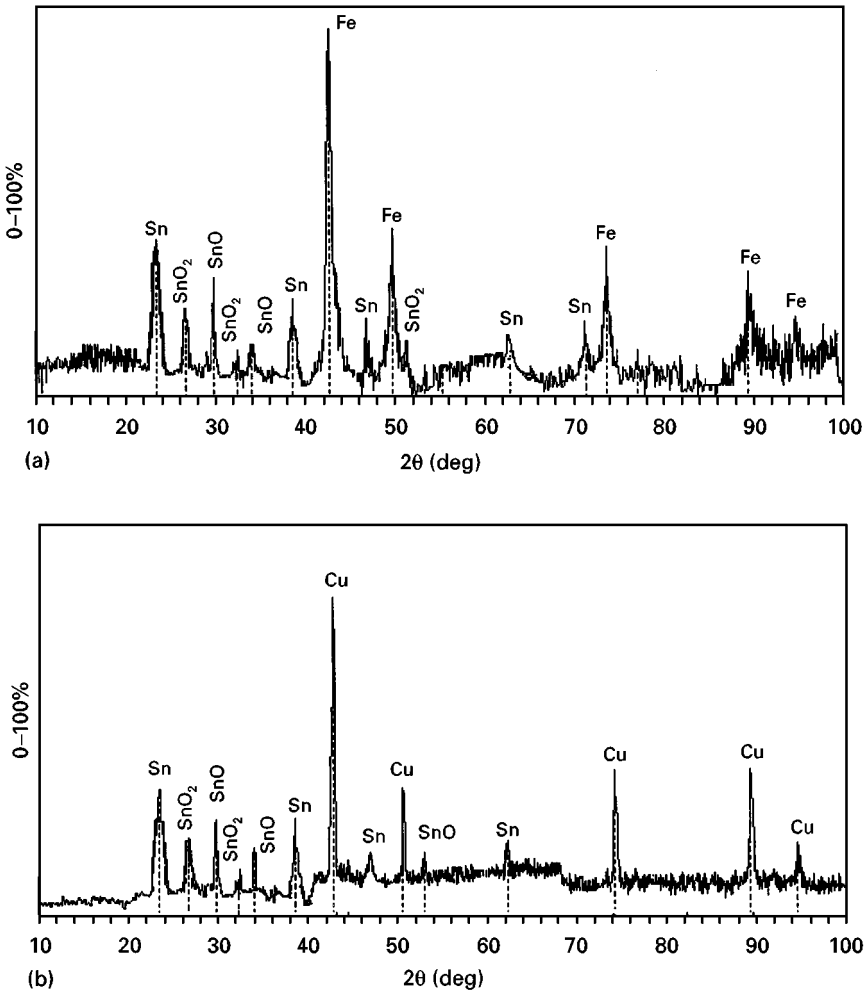


*Figure 6* XRD patterns of Sn-rich tin oxide coatings: (a) Sn on type 304 stainless steel; (b) Sn on a Cu substrate.

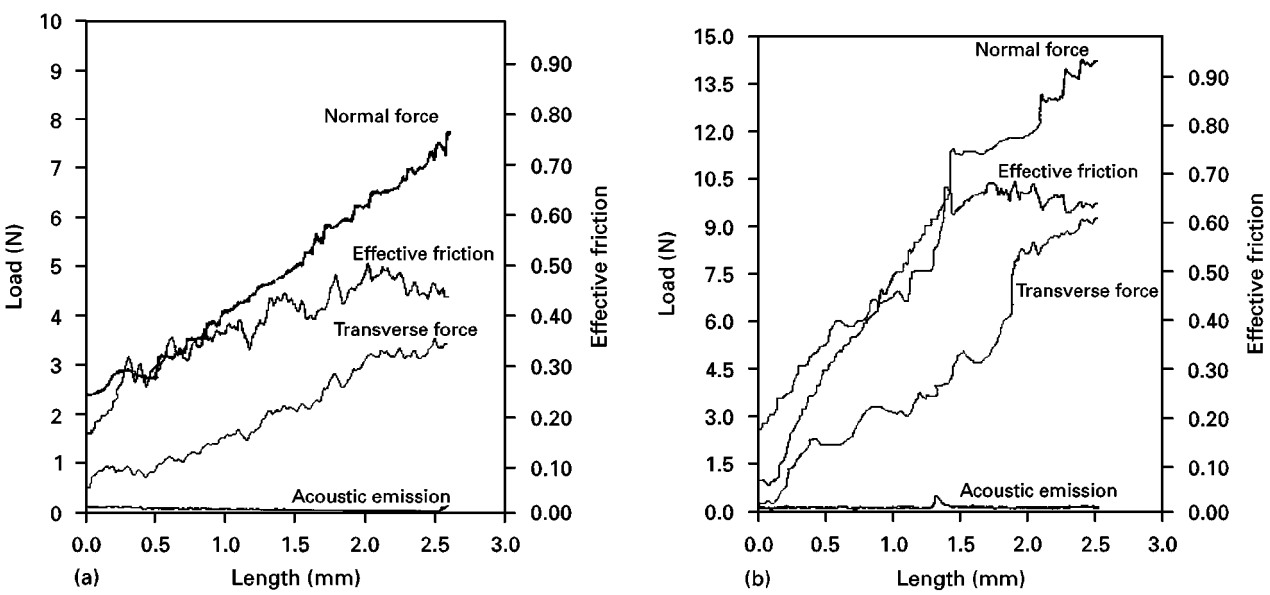


*Figure 7* Load versus scratch length for (a) Cu deposited on Al alloy 6061 and (b) Ni deposited on Al alloy 6061.

reason for this possibly was adsorbed $H_2$ that produces active hydroxide products and helps their desorption from the surface.

There are relatively few reported values of quantitative deposition rates for Cu, Ni and Sn coatings on metal and ceramic substrates. Since Cu coating, by either CVD or MOCVD, has attracted more interest than those of Ni and Sn, only some quantitative depositon rates have been reported for Cu. Moshier *et al.* [23] obtained a 80 nm $min^{-1}$ deposition rate for Cu,

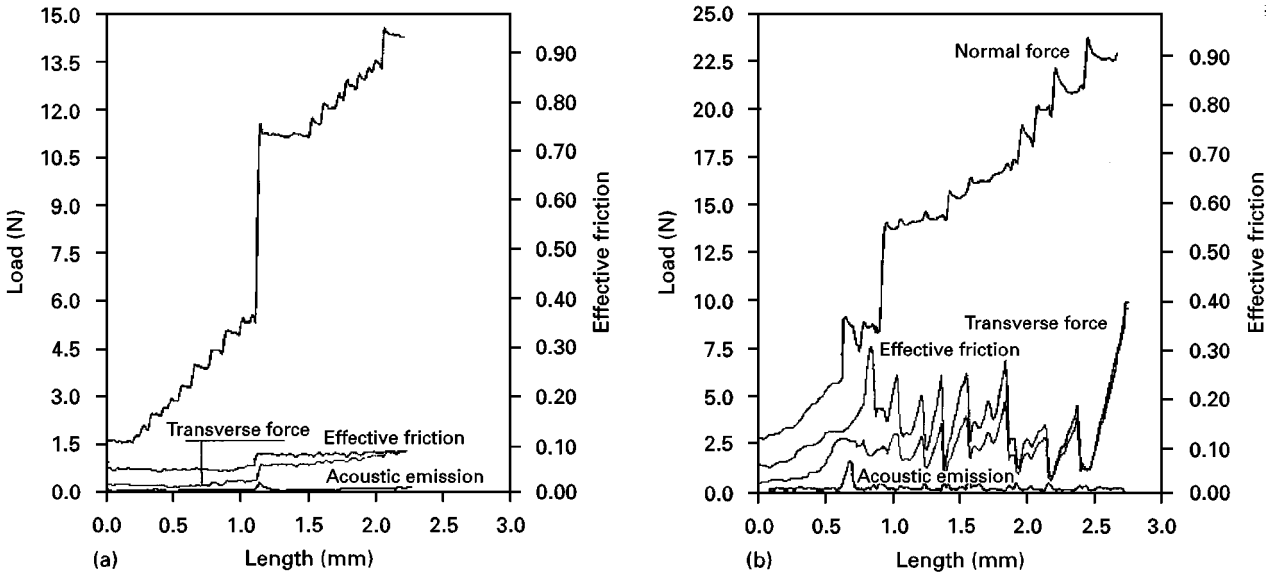


*Figure 8* Load versus scratch length for (a) Ni deposited on a glass microscope slide and (b) Ni deposited on an alumina substrate.

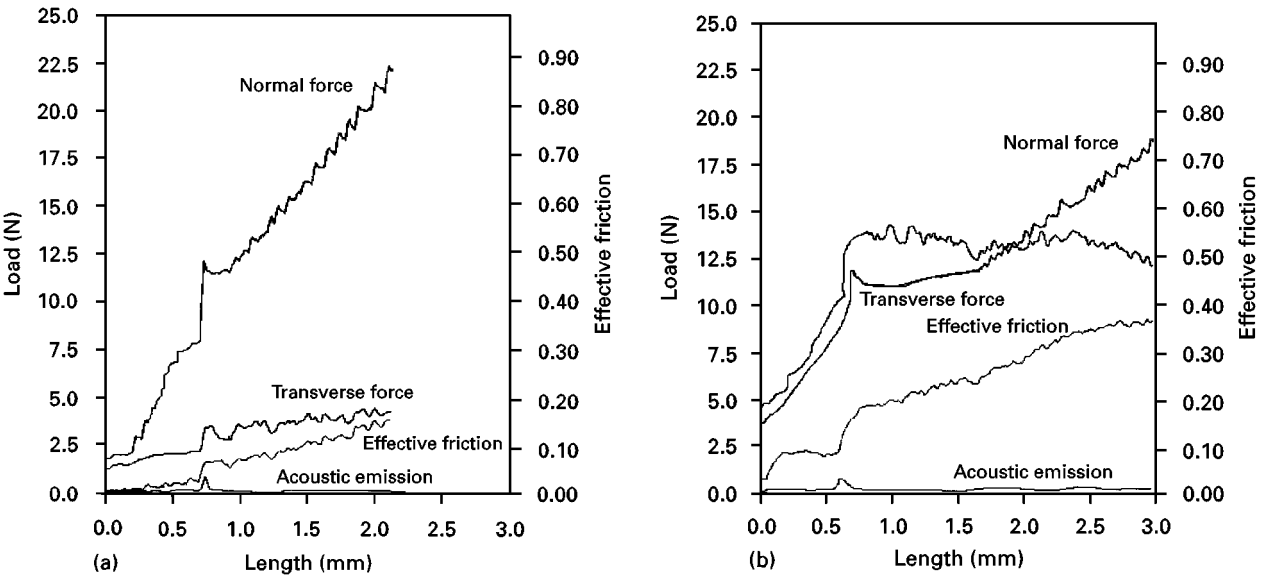


*Figure 9* Load versus scratch length for (a) Sn deposited on type 304 stainless steel and (b) Sn deposited on a Cu substrate.

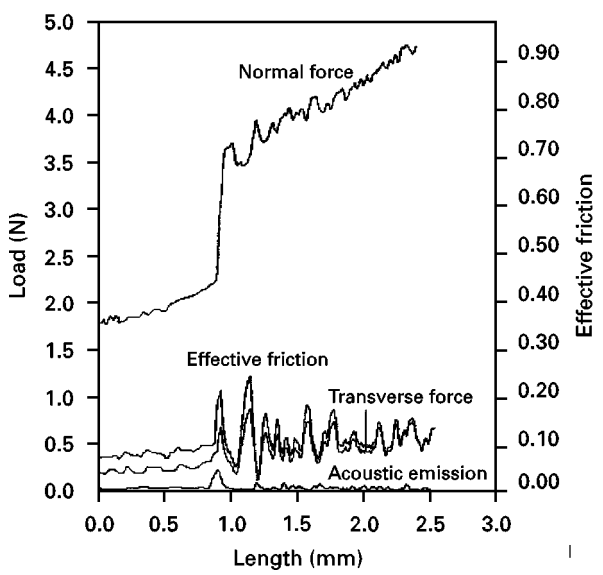


*Figure 10* Load versus scratch length for Ni deposited on an Al alloy 6061 Al substrate by electroless deposition.

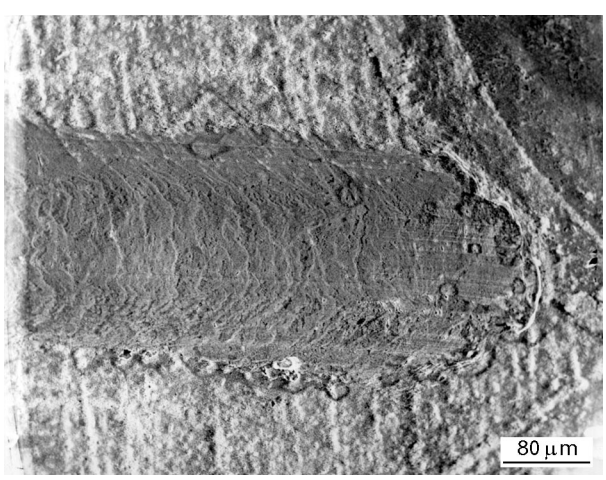


*Figure 11* Scanning electron micrograph of channel produced by moving a 0.553 μm stylus on the Cu-coated Al substrate.

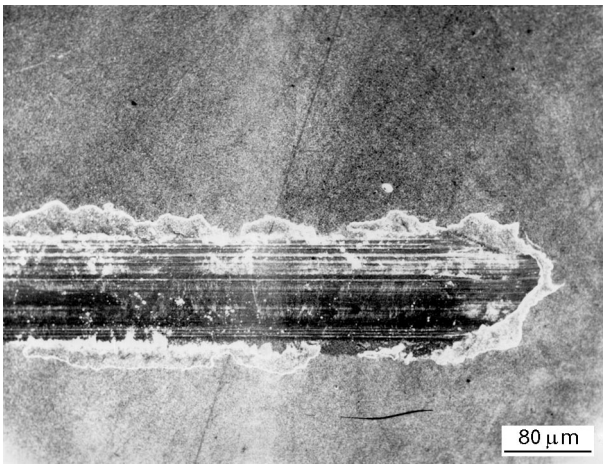


*Figure 12* Scanning electron micrograph of channel produced by moving a 0.553 μm stylus on the Ni-coated glass microscope slide substrate.

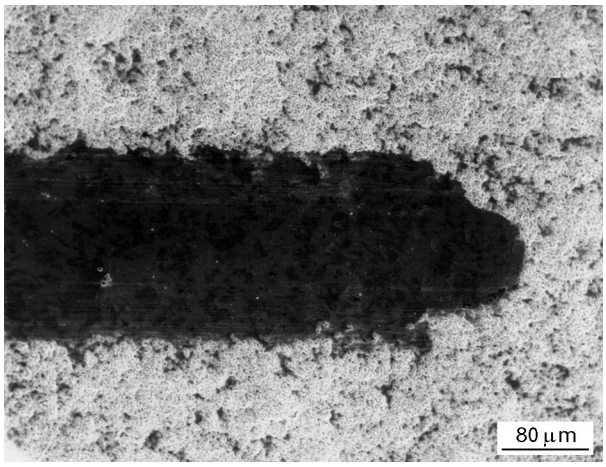


*Figure 14* Scanning electron micrograph of channel produced by moving a 0.553 μm stylus on the Sn-coated 304 stainess steel substrate.

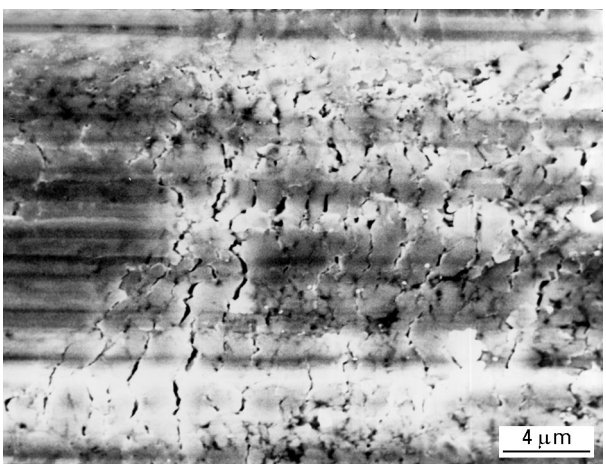


*Figure 13* High magnification of the scratch channel of Ni deposited on the glass substrate, showing cracks after extensive plastic deformation of Ni.

using $Cu(hfc)_2$ precursor. Kaloyeros *et al.* [24] have obtained 120–180 nm $min^{-1}$ depostition rate, whereas Kodas and Smith [3] reported deposition rates of 900 nm $min^{-1}$ at temperatures as low as 200 °C, using $Cu(hfc)_2$. Kim *et al.* [1] have estimated a deposition rate between 2000 and 5000 nm $min^{-1}$ for Cu films by CVD, using $Cu(hfa)_2$ precursor, for a 330 °C substrate temperature. However, Zheng *et al.* [25] found a 2500 nm $min^{-1}$ deposition rate for Cu films grown by β-diketonate source precursor using PACVD, and Gerfin *et al.* [26] reported a 1000 nm $min^{-1}$ deposition rate of Cu films on quartz substrates at a $H_2$ flow rate of 40 $cm^3 s^{-1}$. Additionally, Awaya and Arita [19] reported that the rate for Cu on a silicon substrate, with $H_2$ carrier gas, was increased by the increase in substrate temperature with radio-frequency PACVD. They used an acetyl-acetonato Cu precursor and measured a 8000 nm $min^{-1}$ deposition rate at a total gas pressure of 250 Pa and 400 °C substrate temperature. These data are summarized in Table III.

In the present work, 1500 nm $min^{-1}$ and 750 nm $min^{-1}$ deposition rates were obtained for Cu and Ni coatings, respectively, on Al alloy 6061. These deposition rates are much higher when compared with those of CVD and MOCVD techniques (Table III). Similarly, Ni and Sn deposition rates, on the different substrates, give higher values than those of the other aforementioned techniques. The deposition rate for Ni was increased, by changing the laser power in the LCVD process, but this was at the expense of coating properties such as purity and adhesion to the substrate.

The grain sizes of Cu films, deposited on tungsten and TiN by MOCVD, were found to vary fairly

TABLE III A summary of literature survey, showing deposition of Cu-, Ni and Sn-based coatings on different substrates

| Technique | Substrate | Coating | Thickness | Deposition rate | Reference |
|---|---|---|---|---|---|
| PVD | Glass | Al | 20000 nm | 300–600 nm $min^{-1}$ | [10] |
| PACVD | Al | Cu | 2000 nm | 2000–5000 nm $min^{-1}$ | [30] |
| LCVD | Si–quartz | Ni | 100–500 μm | 0.5–1 μm $min^{-1}$ | [16] |
| CVD | Glass, stainless steel | Cu | 500–800 μm | 80 nm $min^{-1}$ | [24] |
| PACVD | Si, Ti, W | Cu | 8000–20000 nm | 500–10000 nm $min^{-1}$ | [19] |
| MOCVD | Si, TiN | Cu | — | 100 nm $min^{-1}$ | [27] |
| PACVD | Si, Si–Ti, Si–Al, TiN, W | Cu | 44000 | 2500 nm $min^{-1}$ | [25] |
| CVD | $TiSi_2$, $CoSi_2$, Al | Cu | 0.1–1.4 μm | 1000–10000 nm $min^{-1}$ | [1] |
| MOCVD | Quartz, sapphire, Al | Cu | 0.1–0.7 μm | 100–1000 nm $min^{-1}$ | [26] |
| CVD | $SiO_2$ | Cu | — | 900 nm $min^{-1}$ | [3] |
| CVD | Glasses | $SnO_2$ | 300–400 nm | 70 nm $min^{-1}$ | [8] |
| CVD, PVD | Al | $SnO_2$ | 250–300 nm | 12–20 nm $min^{-1}$ | [28] |

linearly with temperature, higher temperatures yielding larger grains [27]. Kodas and Smith [3] insisted that the morphology is strongly affected by the total system pressure. Plan-view image of films grown at atmospheric pressure resembled a layer that showed protrusions to various heights from a rough polycrystalline structure. In contrast, films grown at high pressure were observed to be smooth well-connected polycrystalline layers.

The earliest example of Ni precursor used for CVD is based on the decomposition of $Ni(CO)_4$. However, a major drawback in using $Ni(CO)_4$ is the extreme toxicity of the compound. Because of this toxicity of $Ni(CO)_4$, less toxic compounds, such as $Ni(C_5H_2)_2$ and $Ni(CH_3C_5H_2)_2$, have been studied. In recent years, LCVD has been used for Ni metallization from $Ni(C_5H_2)_2$ and $Ni(CO)_4$ compounds [3]. A few studies have been made on the PACVD of Ni; Jervis [15] used a high-pressure $CO_2$ laser to create an argon plasma above the surface of the substrate. However, AES depth profiling indicated that the composition of the films was 90 at % Ni–9 at % C– 1 at % $O_2$.

Ni coating on glass microscope slides, in the present study, showed uniform coverage of the substrate. No separation of the film from the substrate was possible. Measurement using scratch test gave an $L_c$ of approximately 5.0 N. The adhesion values derived in the plasma assisted coating is approximately four times that of electroless coating, as indicated earlier. The high adhesion strength obtained for Ni on glass is attributed herein to oxidation of Ni on the Ni–glass interface and this leads to the formation of an oxide layer adjacent to the oxides of the substrates. Similar results have been obtained by Laugier [10] on scratch tests of the Al/glass system.

Both thick and thin films of tin oxide are extensively used for resistive gas sensors. Tin-oxide-based coatings are obtained by CVD, PVD, spray pyrolysis and screen printing. Ansari *et al.* [28] have measured a 250 nm $SnO_2$ thickness by CVD and 300 nm by PVD. In the present work, Sn-rich tin oxide (SnO and $SnO_2$) depositions have been obtained in the form of thick layer which are thicker than 6 μm. With the technique used in the present work, it is possible to obtain pure tin, SnO or $SnO_2$ coatings by changing the oxygen partial pressure in the system.

Acoustic emissions are stress waves emitted by sudden localized changes in stress form, i.e., crack formation [28]. As the applied load increases, the acoustic noise level sensed by acoustic transducer increases. The acoustic energy normally increases drastically when one of the following events occur for a soft coating on hard substrates [10, 18].

(i) The transverse strength of non-brittle coatings is exceeded and surface microcracks are generated.
(ii) The non-brittle coating tears from the surface.
(iii) The substrates fail and the diamond dislodges substrate material.

The existence of microcracking does not usually indicate coating failure but merely that the drag force (transverse force) of the diamond has exceeded the lateral tensile strength of the coating. If any abrupt changes are observed in acoustic emission and effective friction, this indicates failure and by reading the *X*-axis intercept, shown in Figs 7–11 associated with this point, the critical load is deduced and reported. The relative value of the critical force of various coatings is a measure of adherence and it varies somewhat as the coating thickness rises. The scratch test results in this study were found to be remarkably high compared with previous investigations in which the coating process included CVD, PVD or MOCVD techniques [29, 30]. The mean critical load values, $L_c$, showed that there is excellent adhesion between coatings and substrates in the coatings generated. As emphasized by Cailler and Lee [30], sputtering of the substrate surfaces obviously led to the increased $L_c$ values measured.

## 5. Conclusions

A combination of PVD and PACVD processes were used to deposit Cu-, Ni- and Sn-rich $SnO/SnO_2$ coatings on metal and ceramic substrates. Coatings were carried out with mixtures of $Ar:H_2$ carrier gas in a d.c. plasma system. A tungsten filament, in the form of crucible and coated with alumina, was used for the evaporation of metal sources. These plasma-assisted metallic coatings on the different metal and ceramic substrates exhibited the following properties.

1. A d.c. plasma source is applicable for coating of pure metals such as Cu and Ni, and metal oxides with the use of a filament used as an evaporator, placed between anode and cathode.
2. A deposition period of 3–5 min is sufficient to obtain coatings with a thickness of approximately 8–10 μm on the metal and ceramic substrates.
3. Oxygen-free deposition of Cu and Ni is achieved even with relatively poor vacuum by the judicious use of hydrogen in the sputtering and deposition gas mixtures. This leads to pure (impurity-free) and uniform coatings.
4. All coatings showed continous smooth polycrystalline structures with a dense surface.
5. The grain sizes of coatings obtained were in the submicron range.
6. Adhesion between deposited layers and substrates is high, possibly emanating from the sputtering–deposition process inherent to this technique.
7. Metal sources can be directly used as precursors in this type of coating technique.
8. The deposition rates are comparatively fast when compared with those of CVD, PVD and MOCVD.

## Acknowledgements

Dr H. Akbulut acknowledges the award of a grant under the NATO Fellowship Program, granted by the Scientific and Technical Research Council of Turkey (TUBITAK).

## References

1. D. H. KIM, R. H. WENTROF and N. G. WILLIAM, *J. Electrochem. Soc.* **140** (1993) 3273.
2. H. N. A. SHAREEF, D. DIMOS, B. A. TUTLE and M. V. RAYMOND, *J. Mater. Res.* **12** (1997) 347.

3. T. KODAS and M. H. SMITH, "The chemisty of metal CVD" (VCH, Weinheim, 1994) pp. 41–203.
4. J. PELLEITER, R. RANTAL and J. C. OBERLIN, *J. Appl. Phys.* **70** (1991) 3862.
5. C. Y. MAK, B. MILLER, L. C. FELDMAN, B. E. WEIR, G. S. HIGASHI, E. A. FITZGERALD, T. BOONE, C. J. DOHERTY and R. B. DOVER, *Appl. Phys. Lett.* **59** (1991) 3449.
6. C. H. J. BREKEL, R. M. M. FONVILLE, P. J. M. STRATEN and G. VERSPUI, in Proceedings of the Eighth International Conference on Chemical Vapour Deposition, 1981, edited by J. M. Blucher, J. R. Batelle, G. E. Vuillard and G. Wahl (Electrochemical Society, Pennington, NJ, 1981) p. 142.
7. G. T. STAUF and P. A. DOWBEN, *Thin Solid Films* **156** (1988) L31.
8. P. MAGUIRE, J. MOLLOY, S. J. LAVERTY and J. McLAUGHLIN *J. Vac. Sci. Tecnol. A* **14** (1996) 3010.
9. S. G. ANSARI, P. BOROOJERDIAN, S. K. KULKARNI, S. R. SAINKAR, R. N. KAREKAR and R. C. AIYAR, *J. Mater. Sci. Mater. Elec.* **7** (1996) 267.
10. M. LAUGIER, *Thin Solid Films* **79** (1981) 15.
11. O. T. INAL and C. V. ROBINO, *ibid.* **95** (1982) 195.
12. S. L. COHEN, M. LIEHR and S. KASI, *Appl Phys. Lett.* **60** (1992) 50.
13. S. J. BULL and D. S. RICKERBY, *Thin Solid Films* **181** (1989) 545.
14. A. G. THOMPSON, *Mater. Lett.* **30** (1997) 255.
15. J. R. JERVIS, *J. Appl. Phys.* **58** (1985) 1400.
16. D. TONNEAU, G. AUVERT and Y. PAULEAU, *ibid.* **66** (1989) 165.
17. S. D. ALLEN and M. BASS. *J. Vac. Sci. Technol.* **16** (1979) 431.
18. C. E. BAUMGARTNER, *J. Amer. Ceram. Soc.* **72** (1989) 890.
19. N. AWAYA and Y. ARITA, *Jpn. J. Appl. Phys.* **30** (1991) 1813.
20. S. P. MURARKA and S. W. HYMES, *Crit. Rev. Solid. Mater. Sci.* **20** (1995) 87.
21. D. TONNEAU, *J. Appl. Phys.* **64** (1988) 5189.
22. S. D. ALLEN, R. Y. JAN, S. M. MAZUK and S. D. VERNON *ibid* **58** (1985) 327.
23. R. W. MOSHIER, R. E. SIEVERS and L. B. SPENDLOVE, US Patent 3 356 527 (1967).
24. A. E. KALOYEROS, A. FENG, J. GARHORT, K. C. BROOKS, S. K. GHOSH, A. N. SEXENA and F. J. MEHERS, *J. Elec. Mater.* **19** (1990) 271.
25. B. ZHENG, E. J. EISENBRAUN, J. LIU and A. E. KALOYEROS, *Appl. Phys. Lett.* **61** (1992) 2175.
26. T. GERGIN, M. BECHT and K. H. DAHMEN, *Mater. Sci. Engng* **B17** (1993) 97.
27. J. A. T. NORMAN, B. A. MURATORE, P. N. DYER, D. A. ROBERTS and A. K. HOCHBERG, *J. Physique IV* **1** (1991) C2-271
28. S. G. ANSARI, S. W. GOSAWI, S. A. GANGAL. R. N. KAREKAR and R. C. AIYER, *J. Mater. Sci. Mater. Elec.* **8** (1997) 23.
29. J. H. JE, E. GYRAMATI and A. NAOUMIDIS, *Thin Solid Films* **136** (1986) 57.
30. M. CAILLER and H. LEE, *ibid.* **168** (1989) 193.

*Received 6 May*
*and accepted 24 September 1997*